ResearchGate

See discussions, stats, and author profiles for this publication at:
https://www.researchgate.net/publication/229188081

Solvation effects on the iodoform ultraviolet direct photodissociation reaction: Opening the photoisomerization channel

ARTICLE *in* CHEMICAL PHYSICS LETTERS · JUNE 2000

Impact Factor: 1.9 · DOI: 10.1016/S0009-2614(00)00561-3

CITATIONS
45

READS
40

2 AUTHORS:

Xuming Zheng
Zhejiang Sci-Tech University
109 PUBLICATIONS **1,259** CITATIONS
SEE PROFILE

David Lee Phillips
The University of Hong Kong
345 PUBLICATIONS **7,029** CITATIONS
SEE PROFILE

Available from: Xuming Zheng
Retrieved on: 23 January 2016

30 June 2000

ELSEVIER

Chemical Physics Letters 324 (2000) 175–182

CHEMICAL PHYSICS LETTERS

www.elsevier.nl/locate/cplett

Solvation effects on the iodoform ultraviolet direct photodissociation reaction: opening the photoisomerization channel

Xuming Zheng, David Lee Phillips *

Department of Chemistry, University of Hong Kong, Pokfulam Road, Hong Kong, China

Received 14 April 2000

Abstract

We present transient resonance Raman spectra that demonstrate that the iso-iodoform photoproduct is mainly associated with the ~400 nm transient absorption band observed following excitation of iodoform in the solution phase. Comparison of our present results with previously reported gas-phase experiments and results for the closely related diiodomethane molecular system suggests that solvation gives rise to noticeable formation of the iso-iodoform photoproduct by some recombination of the initially formed CHI_2 and I photofragments within a solvent cage. © 2000 Elsevier Science B.V. All rights reserved.

1. Introduction

Polyhalomethanes such as diiodomethane and dibromomethane have been commonly used as reagents for cyclopropanation reactions with alkenes [1–8]. Ultraviolet excitation of diiodomethane [2–5] or use of a Zn–Cu couple (in the Simmons–Smith reaction) [1] is used to activate diiodomethane for cyclopropanation reactions. Similarly, use of iodoform with SmI_2 has been reported for diiodomethylation of carbonyl compounds [9]. Polyhalomethanes are also of interest because they may be a significant source of organobromine or organoiodide compounds emitted into the atmosphere [10–15].

There are few reports of experimental work on the ultraviolet (UV) photolysis of iodoform [16–18]. Bersohn and coworkers [16] examined the angular distributions of the photofragments produced by UV photolysis of iodoform in the gas phase. They found that the lower-lying excited states dissociate to give an iodine atom and the CHI_2 radical with the dissociation occurring in a time much shorter than the rotational period of the parent molecule. Photoexcitation (with a 3 ns laser pulse at 347 nm) of iodoform in mesitylene solution leads to formation of an iodine–mesitylene complex immediately after photolysis and indicates that I atoms and CHI_2 radicals are also formed in the solution phase [17]. Pulse radiolysis of iodoform in 1,2-dichloroethane solution gives rise to characteristic transient absorption bands at ~400 nm (intense) and 610 nm (weak) that have been assigned to the iodoform radical cation (CHI_3^+) [18].

In this Letter, we report a nanosecond transient resonance Raman investigation of the iodoform

* Corresponding author. Fax: +852-2857-1586; e-mail: phillips@hkucc.hku.hk

0009-2614/00/$ - see front matter © 2000 Elsevier Science B.V. All rights reserved.
PII: S0009-2614(00)00561-3

photoproducts produced by UV photoexcitation in the solution phase. Our results indicate that iso-iodoform photoproduct is mainly responsible for the characteristic ~400 nm transient absorption band appearing after excitation of iodoform in the solution phase. Comparison of our present results for iodoform with those previously reported for diiodomethane suggests that solvation effects (likely by recombination of the I and CHI_2 fragments within a solvent cage) produces noticeable amounts of the iso-iodoform photoisomerization photoproduct that is observed within nanoseconds after photoexcitation in our transient resonance Raman experiments.

2. Experiment

Iodoform (99%), chloroiodomethane (97%) and spectroscopic grade cyclohexane (99.9 + %) were used to prepare samples (~0.20 M) for the resonance Raman experiments. The apparatus and methods used for the nanosecond time-resolved resonance Raman experiments have been detailed previously [19–21] and only a brief description will be given here. The hydrogen Raman shifted laser lines of the harmonics of a nanosecond pulsed Nd:YAG laser supplied the pump and probe wavelengths for the two-color pump–probe resonance Raman experiments. Pump–probe delays of 0 and 10 ns were used to acquire the transient resonance Raman spectra. The pump and probe laser beams were lightly focused with a near collinear geometry onto a flowing liquid sample and the Raman scattering was collected with reflective optics using a backscattering geometry. The Raman scattered light was imaged through a depolarizer and entrance slit to a 0.5 m spectrograph whose grating dispersed the Raman light onto a liquid nitrogen cooled CCD detector mounted on the exit port of the spectrograph. The Raman signal was accumulated by the CCD for 300–600 s before being read out to an interfaced PC computer and 10–20 of these readouts were summed to get the Raman spectrum. Pump-only, probe-only, pump–probe resonance Raman spectra and a background spectrum were obtained and the known frequencies of the cyclohexane solvent Raman bands were used to calibrate the Raman shifts (in cm^{-1}) of the resonance Raman spectra. Subtraction of the probe-only and pump-only spectra from the pump–probe resonance Raman spectrum was done to remove the solvent and parent compound Raman bands and obtain the transient resonance Raman spectrum.

3. Calculations

The Gaussian program suite (G98W) was used for all of the density functional theory (DFT) calculations reported here [22]. Complete geometry optimization and vibrational frequency calculations were done analytically using a C_1 symmetry. B3LYP computations were done to find the optimized geometry and vibrational frequencies of the species studied. Time-dependent density functional theory at random-phase approximation [23] computations (TD(RPA)) were done to find the electronic transition energies of the species examined. The Sadlej PVTZ basis set [24] was used for all of the DFT calculations.

4. Results and discussion

Fig. 1 presents the UV absorption spectrum of iodoform in cyclohexane solution. The pump and probe wavelengths for the transient resonance Raman experiments are indicated above the absorption spectrum of Fig. 1. The 368.7 nm pump excitation

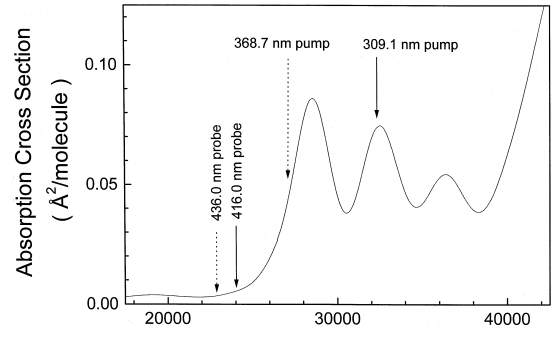

Fig. 1. Absorption spectrum of iodoform in cyclohexane solution with the pump and probe excitation wavelengths for the transient resonance Raman experiments indicated above the spectrum. The 309.1 nm pump wavelength is resonant with the second absorption band and the 368.9 nm pump wavelength is resonant with the first absorption band.

wavelength is resonant with the lowest energy absorption band (~350 nm) and the 309.1 nm excitation wavelength is resonant with the second lowest energy absorption band (~310 nm). The probe wavelengths of 435.9 and 416.0 nm are resonant with the broad transient absorption band ~400 nm observed following excitation of iodoform in solution [18]. Fig. 2 shows a typical pump–probe resonance Raman spectrum, a probe-only resonance Raman spectrum, a pump-only spectrum in the probe wavelength region, and a transient resonance Raman spectrum of the photoproduct species obtained by subtraction of the probe-only spectrum from the pump–probe spectrum. Fig. 3 displays the transient resonance Raman spectra obtained for the product

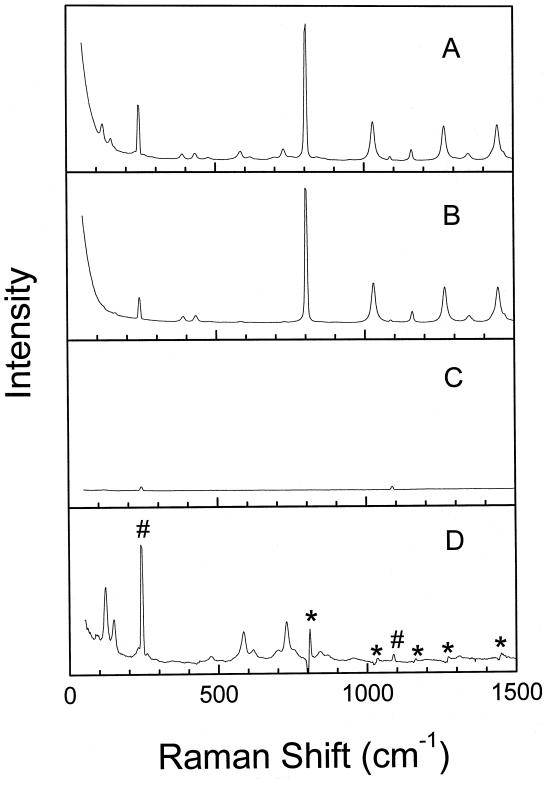

Fig. 2. Examples of a typical pump–probe (A) resonance Raman spectrum, a probe-only (B) resonance Raman spectrum, a pump-only spectrum in the probe wavelength region (C), and a transient resonance Raman spectrum of iso-iodoform (D) obtained by subtracting a probe-only spectrum from the pump–probe spectrum. The asterisks (*) mark regions where solvent subtraction artifacts are present and the pound signs (#) mark stray light artifacts.

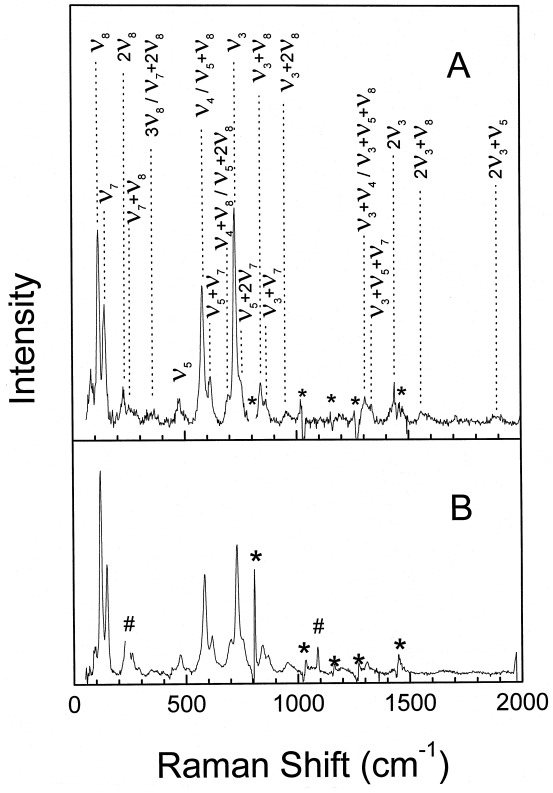

Fig. 3. Transient resonance Raman spectra of iso-iodoform photoproduct produced after photoexcitation within the first absorption band (B) and the second absorption band (A) of iodoform (the pump–probe delay was ~0 ns). The tentative assignments for the Raman bands are indicated above the top spectrum. The asterisks (*) label solvent subtraction artifacts and the pound signs (#) mark stray light artifacts.

species formed after photoexcitation within the first and second absorption bands (the pump–probe delay was ~0 ns). Transient resonance Raman spectra obtained with a pump–probe delay of 10 ns (not shown) were noticeably weaker with lower signal to noise but otherwise were very similar to those obtained with ~0 ns delay (Fig. 2A and Fig. 3). Comparison of the transient resonance Raman spectra of Fig. 3 shows that the same photoproduct species is formed whether the iodoform parent compound is excited in the first absorption band (~350 nm) or in the second absorption band (~310 nm). The transient resonance Raman spectra displayed in Fig. 3 have most of the Raman intensity in the

fundamentals, overtones and combination bands of five Franck–Condon active vibrational modes (726, 579, 477, 144, and 117 cm^{-1}).

We have performed DFT computations to find the optimized geometries, vibrational frequencies, and electronic absorption transitions for the CHI_2, iso-CHI_3 and CHI_3^+ species. Table 1 gives the parameters for the optimized geometries of CHI_2, iso-CHI_3 and CHI_3^+ found from the B3LYP/Sadlej-PVTZ DFT computations. Tables 2 and 3 compares the experimental vibrational frequencies obtained from the transient resonance Raman spectra of Fig. 3 with the calculated vibrational frequencies obtained from the B3LYP/Sadlej-PVTZ computations. Examination of Tables 2 and 3 shows that the resonance Raman fundamental vibrational frequencies are in good agreement with the calculated vibrational frequencies for the iso-CHI_3 species but not with those of the CHI_3^+ radical cation or the CHI_2 radical. For instance, neither the CHI_2 radical or the CHI_3^+ radical cation have two low frequency modes in the 100–200 cm^{-1} region that are associated with the photoproduct observed in the transient resonance Raman spectra (the 117 and 144 cm^{-1} fundamentals). The 117 and 144 cm^{-1} fundamental resonance Raman bands have noticeable intensity in their combination bands with each other and with several other modes (see Fig. 3). The photoproduct transient resonance Raman spectra have three fundamental Raman bands in the 400–750 cm^{-1} region (477, 579, and 726 cm^{-1}) that correspond well to vibrational modes of iso-CHI_3. However, the CHI_2 radical and CHI_3^+ radical cations have only one A_1 or A' vibrational mode in the 400–750 cm^{-1} region. The transient resonance Raman fundamentals observed in the spectra of Fig. 3 and listed in Table 2 are assigned as follows: the 117 cm^{-1} fundamental to the ν_8 nominal I–I stretch, the 144 cm^{-1} fundamental to the ν_7 nominal C–I–I bend, the 477 cm^{-1} fundamental to the ν_5 I–C–I symmetric stretch, the 579 cm^{-1} fundamental to the ν_4 nominal CH wag, and the 726 cm^{-1} fundamental to the ν_3 I–C–I asymmetric stretch. Our results strongly indicate that the characteristic transient absorption band observed $\sim$400 nm following excitation of iodoform in the solution phase is mostly associated with the iso-CHI_3 photoproduct species. Fig. 4 shows a schematic diagram of the structures of iodoform (CHI_3) and iso-CHI_3.

Table 1
Parameters for the optimized geometries computed from the B3LYP DFT calculations for iso-CHI_3, CHI_2, and CHI_3^+ species. Bond lengths are in Å and bond angles are in degrees

Parameter	B3LYP/ Sadlej PVTZ
Iso-CHI_3	
C–I_1	2.000
I_1–I_2	3.036
C–I_3	2.073
C–H_4	1.096
C–I_1–I_2	128.8
I_1–C–I_3	125.9
I_1–C–H_4	115.8
I_3–C–H_4	113.4
CHI_3^+	
C–I_1, C–I_2 and C–I_3	2.145
C–H_4	1.096
I_1–C–I_2, I_1–C–I_3, I_2–C–I_3	111.3
I_1–C–H_4, I_2–C–H_4, I_3–C–H_4	107.6
CHI_2	
C–I_1, C–I_2	2.064
C–H	1.093
I_1–C–I_2	125.1
I_1–C–H and I_2–C–H	117.2
D(I_1–C–H–I_2)	172.4

We have previously used B3LYP/3-21G* TD/RPA computations to find electronic transition energies for the absorption spectra of CH_2I_2 and obtained reasonable agreement with the experimental spectra [25]. Similar computations with larger basis sets (B3LYP/Sadlej-PVTZ) are shown in Table 3 for the allowed singlet electronic absorption transitions of iso-CHI_3, CHI_3^+ radical cation and CHI_2 radical. Inspection of Table 3 shows that iso-CHI_3 has several electronic transitions with significant oscillator strength in the 400–470 nm region (465, 452 and 414 nm with oscillator strengths of $f = 0.5096$, 0.0134, 0.0045). However, the CHI_3^+ radical cation (406 nm with an oscillator strength of 0.0006) and the CHI_2 radical (398 nm with an oscillator strength of $f = 0.0000$) have much weaker calculated transitions. Our assignment of the transient absorption band in the 400 nm region to be mainly due to the iso-CHI_3 species is consistent with the results of the DFT calculated electronic transition energies and oscillator strengths for iso-CHI_3.

How does the UV excitation of iodoform in the solution phase give rise to iso-CHI_3 photoproduct

Table 2
Comparison of the experimental vibrational frequencies (in cm^{-1}) found from the transient resonance Raman spectra (this work) to the calculated B3LYP DFT vibrational frequencies

Vibrational mode		B3LYP/ Sadlej PVTZ	Resonance Raman (this work)
	Iso-CHI_3		
A′	ν_1, CH stretch	3153	
	ν_2, CH scissor	1142	
	ν_3, I–C–I asym. stretch	750	726
	ν_4, CH wag	610	579
	ν_5, I–C–I asym. stretch	478	477
	ν_6, I–C–I bend	155	
	ν_7, C–I–I bend	145	144
	ν_8, I–I stretch	119	117
	ν_9, torsion	29	
	CHI_3^+		
A_1	ν_1, CH stretch	3150	
	ν_2, I–C–I sym. stretch	450	
	ν_3, I–C–I bend	151	
E	ν_4, I–C–H scissor	1075	
	ν_5, I–C–I asym. stretch	580	
	ν_6, I–C–I bend	58	
	CHI_2		
A′	ν_1, CH stretch	3191	
	ν_2, I–C–I sym. stretch	496	
	ν_3, I–C–I bend	131	
	ν_4, CH wag	69	
A″	ν_5, ICH scissor	1114	
	ν_6, I–C–I asym. stretch	708	

sym. = symmetric; asym. = asymmetric; def. = deformation.

we observe in the nanosecond transient resonance Raman spectra? In order to address this question, it is interesting to inspect the closely related di-iodomethane system that has been more extensively

Table 3
Electronic absorption transition energies obtained from DFT calculations for iso-CHI_3, CHI_3^+, and CHI_2. Calculated transition oscillator strengths are in parentheses

Molecule		URPA//UB3LYP/Sadlej PVTZ		
Iso-CHI_3		singlet transitions		
		465 nm (0.5096)		
		452 nm (0.0134)		
		414 nm (0.0045)		
		324 nm (0.1408)		
		293 nm (0.0064)		
CHI_3^+	A_1 to E	1264 nm		
		405 nm (0.0006)		
		322 nm (0.0002)		
	A_1 to A_2	1190 nm		
	A_1 to A_1	327 nm		
CHI_2		398 nm		
		308 nm (0.0000);	301 nm (0.0000);	298 nm (0.0000)
		236 nm (0.0006);	232 nm (0.0068);	227 nm (0.0006)
		218 nm (0.0010);	214 nm (0.0131);	212 nm (0.0381)

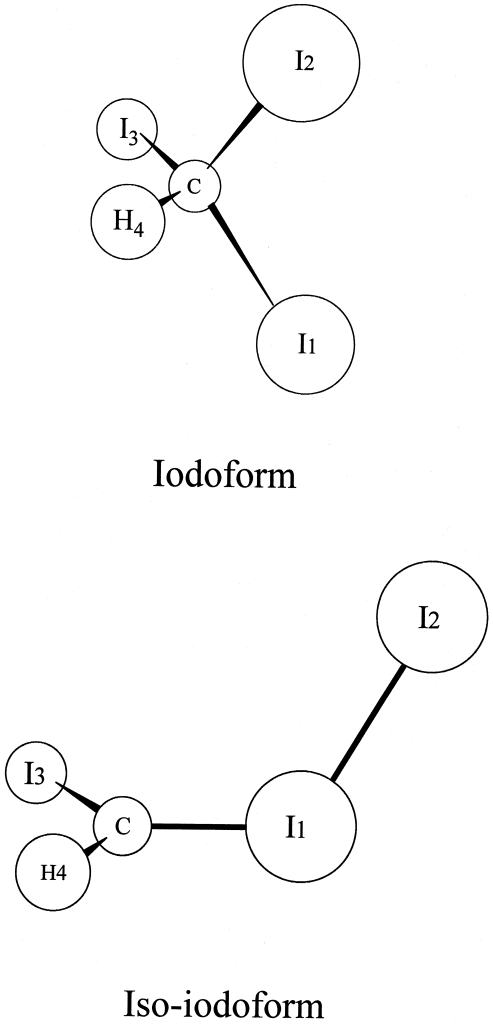

Fig. 4. Schematic diagram of the geometries of iodoform and iso-iodoform.

investigated [26–33]. Ultraviolet excitation of diiodomethane in the gas phase leads to direct C–I bond cleavage (to give CH_2I and I fragments) [16,26–28] similar to CHI_3 in the gas phase (to give CHI_2 and I fragments [16]. Solution phase femtosecond transient absorption experiments for diiodomethane [29–31] have shown that the initial process is also C–I bond cleavage. All three of the femtosecond experiments reported similar results with a fast rise component of a few hundred femtoseconds (ascribed to C–I bond cleavage) followed by a fast decay component of several hundred femtoseconds (due to some geminate recombination) and a slower rise component on the picosecond timescale [29–31]. The interpretation of the femtosecond results varied somewhat due to differing assignments of the species responsible for the transient absorption [29–31]. We recently used nanosecond transient resonance Raman spectroscopy to observe the photoproduct that gives rise to the characteristic ~ 385 nm transient absorption produced following UV photoexcitation of diiodomethane in solution [32]. Our transient resonance Raman spectra with a comparison to results from DFT calculations for proposed photoproduct species and previously reported infrared spectra of dihalomethane isomers observed in low-temperature solids [33] demonstrated that the iso-diiodomethane (CH_2I–I) photoproduct was the species responsible for the ~ 385 nm transient absorption band (at least on the nanosecond timescale). In so far as the transient absorption band ~ 385 nm observed on the ultrafast timescale is the same as that seen on the nanosecond timescale, the basic interpretation of the femtosecond transient absorption experiments by Akesson and coworkers [31] is likely correct: UV photoexcitation of diiodomethane in solution gives rise to fast C–I bond cleavage to form CH_2I and I fragments, these photofragments then collide with the solvent cage to give some recombination to form hot iso-diiodomethane photoproduct that then vibrationally cools to give the iso-diiodomethane observed at later times. Recombination of the CH_2I and I photofragments within the solvent cage apparently leads to significant production of iso-diiodomethane photoproduct following UV excitation of diiodomethane in room-temperature solutions. It is probable that a similar mechanism leads to formation of the iso-CHI_3 photoproduct that we observe following UV excitation of solution phase iodoform (CHI_3).

We note that photoexcitation of iodoform in either the A-band (~ 350 nm) or the B-band (~ 310 nm) leads to the same iso-iodoform product being observed in the nanosecond transient resonance Raman spectra. This suggests that the formation of the iso-iodoform photoproduct is not specific to a particular transition but probably occurs in general for $n \rightarrow \sigma^*$ transitions localized on C–I bonds for polyiodomethanes. Photoisomerization photoproducts were observed for several dihalomethanes

subsequent to UV excitation in low-temperature solid matrices where the more rigid solid environment would be expected to provide very efficient caging of the initially produced photoproducts [33]. The iso-dihalomethane species thermal stabilities were measured in the solid-state experiments [33] and iso-diiodomethane disappears above 100 K and other iso-dihalomethane species (like iso-bromoiodomethane and iso-chloroiodomethane) had much lower stabilities. Thus, it was not clear whether the iso-dihalomethane species would have any importance for reactions taking place in room-temperature liquid solutions. Our recent observation of the iso-diiodomethane photoproduct [32] and iso-CHI_3 photoproduct (this work) following UV excitation of diiodomethane and iodoform in room-temperature liquid solutions suggests that sufficient solvent caging of the initially formed photodissociation fragments occurs in room-temperature liquid solutions so that noticeable amounts of iso-polyhalomethane photoproducts can be produced.

We attempted identical experiments for chloroiodomethane (273.9 nm pump and 416.0 nm probe and several other wavelength combinations) in cyclohexane solution and observed no iso-chloroiodomethane signal in the resonance Raman experiments although this species could easily be detected in the low-temperature solid-state experiments [33]. This could be due to several factors: the iso-chloroiodomethane species is much more unstable and/or the solvent caging is much less efficient for the chloroiodomethane photofragements. The lighter and smaller chloromethyl radical (CH_2Cl) likely has more of the available energy from photodissociation in translation and would be expected to have more efficient solvent cage escape than the heavier and larger iodomethyl (CH_2I) and CHI_2 radicals that have less energy partitioned to translation from the photodissociation [16]. Our present results for iodoform (iso-idodoform readily observed) and chloroiodomethane (no iso-chloroiodomethane observed) indicate that the solvent caging in room-temperature liquids is significantly different than that found for the more rigid low-temperature solid matrices [33].

The details of the mechanism of the formation of iso-polyhalomethane photoproducts in room-temperature solutions could be directly investigated using ultrafast time-resolved experiments (like transient absorption and/or vibrational spectroscopies) similar to studies done for diiodomethane [29–31]. Such studies would be attractive for investigating solvent–solute interactions and solvent-induced caging effects on photodissociation/photoisomerization reactions in condensed-phase environments. It would also be interesting to do similar studies in low-temperature solid-state matrix environments to compare with the liquid solution results.

Acknowledgements

This work was supported by grants from the Committee on Research and Conference Grants (CRCG), the Research Grants Council (RGC) of Hong Kong, the Hung Hing Ying Physical Sciences Research Fund and the Large Items of Equipment Allocation 1993-94 from the University of Hong Kong.

References

[1] H.E. Simmons, R.D. Smith, J. Am. Chem. Soc. 81 (1959) 4256.
[2] D.C. Blomstrom, K. Herbig, H.E. Simmons, J. Org. Chem. 30 (1965) 959.
[3] N.J. Pienta, P.J. Kropp, J. Am. Chem. Soc. 100 (1978) 655.
[4] P.J. Kropp, N.J. Pienta, J.A. Sawyer, R.P. Polniaszek, Tetrahedon 37 (1981) 3229.
[5] P.J. Kropp, Acc. Chem. Res. 17 (1984) 131.
[6] E.C. Friedrich, J.M. Domek, R.Y. Pong, J. Org. Chem. 50 (1985) 4640.
[7] E.C. Friedrich, S.E. Lunetta, E.J. Lewis, J. Org. Chem. 54 (1989) 2388.
[8] S. Durandetti, S. Sibille, J. Périchon, J. Org. Chem. 56 (1991) 3255.
[9] J.M. Concellón, P.L. Bernad, J.A. Pérez-Andrés, Tetrahedron Lett. 39 (1998) 1409.
[10] Th. Class, K. Ballschmiter, J. Atmos. Chem. 6 (1988) 35.
[11] S. Klick, K. Abrahamsson, J. Geophys. Res. 97 (1992) 12683.
[12] K.G. Heumann, Anal. Chim. Acta 283 (1993) 230.
[13] R.M. Moore, M. Webb, R. Tokarczyk, R. Wever, J. Geophys. Res. Oceans 101 No. C 9 (1996) 20899.
[14] L. Carpenter, East Atlantic Spring Experiment (EASE) (1997 campaign).
[15] J.C. Mössigner, D.E. Shallcross, R.A. Cox, J. Chem. Soc. Faraday Trans. 94 (1998) 1391.

[16] M. Kawasaki, S.J. Lee, R. Bersohn, J. Chem. Phys. 63 (1975) 809.
[17] A. Van den Emde, S. Kimel, S. Speiser, Chem. Phys. Lett. 21 (1973) 133.
[18] H. Mohan, P.N. Moorthy, J. Chem. Soc. Perkin Trans. 2 (1990) 277.
[19] L.C.T. Shoute, D.-H. Pan, D.L. Phillips, Chem. Phys. Lett. 290 (1998) 24.
[20] D.-H. Pan, D.L. Phillips, J. Phys. Chem. A 103 (1999) 4737.
[21] D. Pan, L.C.T. Shoute, D.L. Phillips, J. Phys. Chem. A 103 (1999) 6851.
[22] M.J. Frisch et. al., GAUSSIAN 98 (Revision A.1), Gaussian, Inc., Pittsburgh, PA, 1998.
[23] A.J. Sadlej, Theor. Chim. Acta 81 (1992) 339.
[24] R. Bauernschmitt, R. Ahlrichs, Chem. Phys. Lett. 256 (1996) 454.
[25] X. Zheng, D.L. Phillips, Chem. Phys. Lett. 316 (2000) 524.
[26] P.M. Kroger, P.C. Demou, S.J. Riley, J. Chem. Phys. 65 (1976) 1823.
[27] G. Schmitt, F.J. Comes, J. Photochem. 14 (1980) 107.
[28] K.W. Jung, T.S. Ahmadi, M.A. El-Sayed, Bull. Korean Chem. Soc. 18 (1997) 1274.
[29] B.J. Schwartz, J.C. King, J.Z. Zhang, C.B. Harris, Chem. Phys. Lett. 203 (1993) 503.
[30] K. Saitow, Y. Naitoh, K. Tominaga, K. Yoshihara, Chem. Phys. Lett. 262 (1996) 621.
[31] A.N. Tarnovsky, J.L. Alvarez, A.P. Yartsev, V. Sundström, E. Åkesson, Chem. Phys. Lett. 312 (1999) 121.
[32] X. Zheng, D.L. Phillips, J. Phys. Chem. A 104 (2000).
[33] G. Maier, H.P. Reisennauer, J. Hu, L.J. Schaad, B.A. Hess Jr., J. Am. Chem. Soc. 112 (1990) 5117.